

Chapter 6 Coherence cloning using OPLLs

6.1 Introduction

Ultra-stable lasers with narrow linewidth and long coherence length are required for applications such as various types of interferometric sensing, Doppler LIDAR, gas detection, frequency metrology, RF signal generation, and coherent communications[4, 40, 69, 70]. The requirement of the linewidth could vary from MHz to sub Hz, depending on the particular application. For the short distance fiber optical sensing, linewidths of a few kHz might be enough. For ground based or space borne gravitational wave detection (VIRGO, LIGO) [71], or RF reference signal distribution in large radiotelescope arrays (ALMA) [71], accurate measurement of tens to millions of km with a resolution of sub micrometer requires the laser to have a sub-Hz linewidth[71].

To achieve a narrow linewidth, an extended optical cavity with very high quality factor is usually used. For example, gas lasers, solid state lasers or fiber lasers with long cavity can have linewidth of a few kHz [72]. Electrical feedback can also be used to further narrow the linewidth of the laser. Very stable Fabry-Perot intefereometers with very high finesse, or the narrow absorption lines of certain gases have been used as frequency discriminators to detect and reduce a laser's frequency noise over a limited frequency bandwidth[40, 70]. Using this approach, lasers with linewidths of sub-Hz have been demonstrated for precision frequency standard synthesis with optical clocks[30, 31]. However these lasers are typically bulky and very expensive due to the complexity of the frequency stabilizing system.

Semiconductor lasers typically have linewidth of between a few hundred kHz and a few MHz due to the low reflectivity of the laser waveguide facet and the linewidth broadening effect[73-76]. Using optical feedback from an external cavity, their linewidths can be reduced to a few kHz. However, the long laser cavity makes it more challenging to achieve stable single frequency operation, and a great deal of effort is necessary for packaging to mechanically isolate the cavity. The linewidth of SCLs has also been

reduced with the electric feedback approach using either a Fabry-Perot interferometer or the absorption line of gases[40, 70]. No matter which approach is used, the advantages of SCLs such as their small size and low cost are lost.

In an ideal OPLL, the slave laser tracks the phase of the master laser instantaneously and thus inherits the coherence property of the master laser. It only takes low cost SCLs and electronic circuits to make OPLLs, which provides an economic way of cloning the superior coherence property of an expensive master laser. This could be very attractive for applications where a large number of coherent laser sources are needed.

Another advantage of heterodyne OPLL is the additional flexibility of controlling the frequency of the slave laser by using an RF offset signal. Once a fixed frequency standard is established, e.g., using a gas absorption line or an optic clock, a tunable narrow linewidth laser source can be made using the heterodyne OPLL technology. A frequency tuning range of up to 100GHz can be achieved with the state-of-the-art RF electronics[21].

In this chapter I will study the cloning of the coherence of a narrow linewidth laser to inexpensive off-the-shelf commercial SCLs with the OPLLs. I will first summarize the description of the frequency stability and the coherence of a single frequency laser. Different experimental methods of characterizing the frequency stability will also be discussed. Afterwards I shall give the theoretical calculation of the frequency or phase noise, the Allan deviation, the degree of coherence, and the lineshape of a SCL phase locked to a cleaner master laser. Finally the experimental measurements will be presented and discussed.

6.2 Phase noise and frequency stability of a single frequency laser

6.2.1 Phase and frequency fluctuations of an oscillator

The optical field of a single frequency laser is modeled as a quasimonochromatic field

$$E(t) = E_0 \exp j[2\pi\nu_0 t + \phi(t)] \quad (6.1)$$

where ν_0 is the average optical frequency and $\phi(t)$ is the phase fluctuation. The intensity noise is not considered here because in semiconductor lasers its integrated power is much smaller than that of the phase noise.

The frequency stability of a laser can be characterized in both the time domain and the frequency domain. In the time domain, traditionally two random variables are widely used to characterize the frequency stability of an oscillator. They are the fractional phase fluctuation $x(t)$ and the fractional frequency fluctuation $y(t)$, which are defined as[77]

$$x(t) = \frac{\phi(t)}{2\pi\nu_0} \quad \text{and} \quad y(t) = \frac{\dot{\phi}(t)}{2\pi\nu_0} \quad (6.2)$$

Note that $x(t)$ also represents the time jittering of the clock signal described by Eq. (6.1). The absolute phase fluctuation is related to $x(t)$ by $\phi(t) = 2\pi\nu_0 x(t)$ and the absolute frequency fluctuation is $\dot{\phi}(t)/2\pi = \nu_0 y(t)$.

6.2.2 Power spectral density of the phase or frequency fluctuation

In actual experimental measurement people typically measure the single-sided power spectral density (PSD) of the fractional frequency fluctuation, i.e. , $S_y(f)$. The PSD of the fractional phase fluctuation, the absolute phase fluctuation, and the absolute frequency fluctuation are related to $S_y(f)$ by

$$S_x(f) = \frac{S_y(f)}{(2\pi f)^2}, \quad S_\phi(f) = (2\pi\nu_0)^2 S_x(f), \quad S_\nu(f) = \nu_0^2 S_y(f) \quad (6.3)$$

Actual experimental practice shows that the single-sided PSD of the fractional frequency fluctuations in most oscillators generally takes a polynomial form[2, 78]

$$S_y(f) = \sum_{\alpha=-2}^2 h_\alpha f^\alpha \quad (6.4)$$

with

- $\alpha=2$: white phase noise
- $\alpha=1$: flicker phase noise
- $\alpha=0$: white frequency noise
- $\alpha=-1$: flicker frequency noise
- $\alpha=-2$: random walk frequency noise

Depending on the detailed composition of an oscillator, the PSD of the frequency fluctuation can have a few non-zero polynomial components. Low values of “a” have not been clearly identified yet because of experimental difficulties related to very long term data acquisition and to the control of experimental conditions for long time. In practice the finite duration of measurements introduces a low frequency cutoff which prevents the divergence of $S_y(f)$ as $f \rightarrow 0$ for $a < 0$. Furthermore, low pass filtering is always present in the measuring instruments, which ensures convergence conditions at the higher-frequency side of the power spectrum.

Experimental studies of the power spectral density of frequency noise and the lineshape have shown that the main contributions in single-mode semiconductor lasers are the white frequency noise due to spontaneous emission, and the $1/f$ flicker noise due to the fluctuation of charge carriers[32, 79-82]. The white frequency noise leads to the well known Lorentzian lineshape and the presence of the $1/f$ noise leads to a Voigt profile resulting from the convolution of a Lorentzian lineshape with a Gaussian lineshape[32, 80]. The $1/f$ noise dominates at low frequency and becomes pronounced only in measurements of long duration. In the following theoretical description I only consider the white frequency noise for the sake of simplicity.

6.2.3 Autocorrelation, coherence and linewidth of an optical field

The autocorrelation of the field and its temporal coherence are very important concepts widely used in many interferometric measurements. The optical field autocorrelation function is a measurement of the coherence between an optical signal and the delayed

version of itself, i.e.,

$$G_E^{(1)}(\tau) = \langle E^*(t)E(t+\tau) \rangle = \langle \exp[j\Delta\phi(t,\tau)] \rangle \exp(j\omega_0\tau) \quad (6.5)$$

where τ is the delay time, $\Delta\phi(t,\tau) = \phi(t+\tau) - \phi(t)$ is the phase jitter between time t and $t+\tau$, and $\langle \rangle$ represents averaging over infinite time. The Fourier transform of $G_E^{(1)}(\tau)$ gives the spectrum, or the lineshape, of the optical field.

In general it is very difficult to calculate the field autocorrelation function given by Eq. (6.5). For the spontaneous emission induced quantum phase noise, the phase jitter $\Delta\phi(t,\tau)$ is assumed to be a zero-mean stationary random Gaussian process[83-86]. With this assumption, one can use the well known relation [87]

$$\langle \exp[\pm j\Delta\phi(t,\tau)] \rangle = \exp\left[-\frac{\langle \Delta\phi^2(\tau) \rangle}{2}\right] \quad (6.6)$$

and the laser field autocorrelation function is simplified to

$$G_E^{(1)}(\tau) = \exp\left[-\frac{1}{2}\langle \Delta\phi^2(\tau) \rangle\right] \exp(j\omega_0\tau) \quad (6.7)$$

The absolute value of $G_E^{(1)}(\tau)$ as a function of τ can be used to measure the degree of coherence of an optical field. The mean square phase jitter $\langle \Delta\phi^2(\tau) \rangle$ is related to the single-sided frequency noise spectrum $S_\nu(f)$ by[87]

$$\langle \Delta\phi^2(\tau) \rangle = 4 \int_0^{+\infty} \sin^2(\pi f\tau) S_\nu(f) \frac{df}{f^2} \quad (6.8)$$

Next I will use two examples to illustrate how the degree of coherence and the lineshape of the field can be obtained from the PSD of the frequency fluctuation.

6.2.4 Example: white frequency noise

White frequency noise due to spontaneous emission is the primary noise source in semiconductor lasers. The corresponding single-sided PSD is $S_\nu(f) = \Delta f / \pi$ [39, 73, 84],

leading to the mean square phase jitter $\langle \Delta\phi^2(\tau) \rangle$ increasing linearly with the delay τ

$$\langle \Delta\phi^2(\tau) \rangle = 2\pi\Delta f |\tau| \quad (6.9)$$

where Δf is the FWHM of the laser spectrum. Substituting Eq. (6.9) into Eq. (6.7), the degree of coherence is simply an exponentially decaying function

$$|G_E^{(1)}(\tau)| = \exp[-\pi\Delta f \tau] \quad (6.10)$$

By taking the Fourier transform of the autocorrelation function, the normalized lineshape corresponding to the white frequency noise exhibits the well known Lorentzian shape

$$S_E(f) = \frac{\Delta f / 2\pi}{(\Delta f / 2)^2 + (f - f_0)^2} \quad (6.11)$$

6.3 Experimental methods of measuring the frequency stability

The experimental characterization of the frequency stability or coherence of a single frequency laser can be conducted both in the time domain and the frequency domain. In the time domain, a frequency counter can be used to record the beat note between two independent lasers, where either the reference laser has significantly lower noise than the device under test, or both lasers have similar performance. This method can achieve very high resolution. However, it requires a second laser and can be inconvenient. In the frequency domain, one can convert frequency fluctuations into intensity fluctuations using a frequency discriminator, such as an unbalanced Mach Zehnder interferometer or a high-finesse reference cavity[38]. By measuring the PSD of the resultant intensity fluctuations, one obtains the PSD of the frequency fluctuations. The linewidth or lineshape of the optical field is another indicator of the coherence of a single frequency laser. To measure the linewidth or lineshape, one often uses the delayed self-heterodyne interferometer (DSHI) technique, which involves measuring the beat note between the

laser output and a frequency-shifted and delayed version of itself.

6.3.1 Time domain measurement of the frequency fluctuation

Assuming that a frequency counter is used to measure the fractional frequency averaged over time interval $[t_k, t_k + \tau]$

$$\bar{y}_k = \frac{1}{\tau} \int_{t_k}^{t_k + \tau} y(t') dt' \quad (6.12)$$

If the time interval between two consecutive measurements is T , the N -sample variance of \bar{y}_k will be

$$\sigma_y^2(N, T, \tau) = \frac{1}{N-1} \sum_{k=0}^{N-1} \left(\bar{y}_k - \frac{1}{N} \sum_{k=0}^{N-1} \bar{y}_k \right)^2 \quad (6.13)$$

The dependence of the expectation value of the N -sample variance on the number of samples N , the sample time τ , and the power spectral density has been considered by Allan[88]. It can be shown that the computation of the average of the N -sample variance introduces a filtering of the PSD $S_y(f)$ [77]

$$\langle \sigma_y^2(N, T, \tau) \rangle = \int_0^{\infty} S_y(f) |H(f)|^2 df \quad (6.14)$$

where $H(f)$ is the transfer function of a linear filter

$$H(f) = \frac{N}{N-1} \left[\frac{\sin \pi f \tau}{\pi f \tau} \right]^2 \left\{ 1 - \left[\frac{\sin \pi f N T}{N \sin \pi f T} \right]^2 \right\} \quad (6.15)$$

The expectation value of the two-sample variance without dead time, i.e., $N = 2$ and $T = \tau$, is called the Allan variance and is generally accepted as the measure of frequency stability in the time domain. One sets

$$\begin{aligned} \sigma_y^2(\tau) &= \langle \sigma_y^2(2, \tau, \tau) \rangle = \frac{1}{2} \langle (\bar{y}_{k+1} - \bar{y}_k)^2 \rangle \\ &= 2 \int_0^{\infty} S_y(f) \frac{\sin^4(\pi f \tau)}{(\pi f \tau)^2} df \end{aligned} \quad (6.16)$$

The square root of the Allan variance is called the Allan deviation $\sigma_y(\tau)$.

The Allan deviation is useful for characterizing a frequency source because of the type of phase noise present is revealed by the dependence of $\sigma_y(\tau)$ on τ . For example, for white frequency noise, $\sigma_y(\tau) \propto \tau^{-1/2}$. For the Allan deviation to reliably reflect the type of noise present, it is crucial that there should be no dead time between consecutive average frequency measurements used to determine $\sigma_y(\tau)$.

6.3.2 Frequency domain measurement

In this section I introduce the different methods of measuring the frequency fluctuation and lineshape of lasers in the frequency domain.

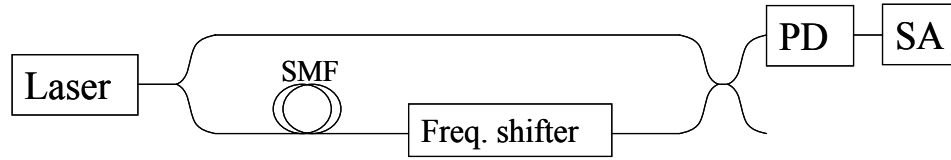


Fig.6.1 Schematic diagram of the delayed self-heterodyne interferometer lineshape measurement setup

Fig. 6.1 gives a schematic diagram of the delayed self-heterodyne interferometer setup. The delay line must be longer than the coherence length of the laser to measure the lineshape. It can also be used as a frequency discriminator to measure the frequency noise spectrum if the delay is kept much shorter than the coherence length and the frequency shifter is removed. Assume the detected total field is a superposition of a laser field $E(t)$ expressed by Eq. (6.1) with a time-delayed and frequency-shifted image of itself[89]

$$E_T(t) = E(t) + \alpha E(t + \tau_0) \exp j2\pi\Omega t \quad (6.17)$$

α is a real factor which accounts for the amplitude ratio between the two mixed fields, Ω is the mean frequency difference between the two mixed fields.

The photo current is proportional to the optical field intensity. Assuming stationary fields, to find the spectrum of the photo current, one can calculate the autocorrelation function of the photocurrent

$$R_I(\tau) = e\eta G_{E_T}^{(2)}(0)\delta(\tau) + \eta^2 G_{E_T}^{(2)}(\tau) \quad (6.18)$$

where e is the electronic charge, η is the detector sensitivity, and $G_{E_T}^{(2)}(\tau)$ is the second-order optical field correlation function defined as

$$G_{E_T}^{(2)}(\tau) = \langle E_T(t)E_T^*(t)E_T(t+\tau)E_T^*(t+\tau) \rangle \quad (6.19)$$

The first term in Eq. (6.18) is the shot noise associated with the DC component of the photocurrent.

6.3.2.1 Power spectral density of the frequency noise

A rigorous analysis of the output of a homodyne frequency discriminator can be obtained by taking the Fourier transform of Eq. (6.19), which is studied in detail in [89]. It involves multiple integrations and is numerically complicated to calculate. A much simpler relation between the photocurrent spectrum and the laser frequency noise spectrum can be found if certain requirements are met.

Assuming that the mixed fields have the same amplitudes, and ignoring the shot noise, the photocurrent generated by the photodetector at one output of the homodyne FM discriminator is[38]

$$I = \eta E_T E_T^* = \eta E_0^2 \left\{ 2 + 2 \cos \left[\omega_0 \tau_0 + \Delta\phi(t, \tau_0) \right] \right\} \quad (6.20)$$

where ω_0 is the average frequency of the optical field and τ_0 is the differential delay of the interferometer. The interferometer is typically biased at the quadrature point $\omega_0 \tau_0 = 2\pi N \pm \pi/2$ where the frequency discrimination sensitivity is the highest. If the phase jitter is small $\Delta\phi(t, \tau_0) \ll 1$, Eq. (6.20) can be simplified to

$$I \approx \pm 2\eta E_0^2 \Delta\phi(t, \tau_0) \quad (6.21)$$

Taking the Fourier transform of Eq. (6.21), the relation between the photocurrent spectrum and the frequency noise spectrum is found to be

$$S_I(f)/(2\eta E_0^2)^2 = 4\pi^2 \tau_0^2 \text{sinc}^2(f\tau_0) S_\nu(f) \quad (6.22)$$

where $\text{sinc}(x) = \sin \pi x / \pi x$. For frequencies much smaller than the free spectral range of the interferometer, i.e., $f\tau_0 \ll 1$, $\text{sinc}^2(f\tau_0) \approx 1$ and $S_I(f)$ is proportional to $S_\nu(f)$. Thus the spectrum of the photocurrent is a direct measurement of the frequency noise spectrum of the laser. The sensitivity of the interferometer is proportional to τ_0 . Therefore a long delay time τ_0 is preferred as long as it satisfies $f\tau_0 \ll 1$ in the frequency range of interest.

6.3.2.2 Self-delayed heterodyne measurement of the lineshape

In the case of the self-delayed heterodyne lineshape measurement, following Eq. (6.19) the second-order optical field autocorrelation function is [89]

$$G_{E_r}^{(2)}(\tau)/E_0^4 = \left[(1 + \alpha^2)^2 + 2\alpha^2 \cos(2\pi\Omega\tau) \cdot \exp(-A) \right] \quad (6.23)$$

where A is

$$A = \langle \phi^2(\tau) \rangle + \langle \phi^2(\tau_0) \rangle - \langle \phi^2(\tau + \tau_0) \rangle / 2 - \langle \phi^2(\tau - \tau_0) \rangle / 2 \quad (6.24)$$

If the spectrum of the frequency noise is known, the mean-square phase jitter $\langle \Delta\phi^2(\tau) \rangle$ and thus the autocorrelation of the photocurrent can be calculated using Eq. (6.8) and Eq. (6.23). As an example, for white frequency noise, one can plug Eq. (6.9) in Eq. (6.23) to get

$$\frac{G_{E_r}^{(2)}(\tau)}{E_0^4} = (1 + \alpha^2)^2 + 2\alpha^2 \cos \Omega\tau \cdot \exp \begin{cases} -|\tau| & \text{for } |\tau| < \tau_0 \\ -|\tau_0| & \text{for } |\tau| > \tau_0 \end{cases} \quad (6.25)$$

Assuming that the mixed signals have equal amplitudes, i.e. $\alpha = 1$ and ignoring the shot noise term, the spectrum of the photocurrent is obtained by taking the Fourier transform of Eq. (6.25)

$$\frac{S_I(f)}{\eta^2 E_0^4} = 4\delta(f) + \exp(-2\pi\Delta f \tau_0) \cdot \delta(f - \Omega) + \frac{\Delta f / \pi}{\Delta f^2 + (f - \Omega)^2} \cdot \left\{ 1 - \exp(-2\pi\Delta f \tau_0) \cdot \left[\cos 2\pi(f - \Omega)\tau_0 + \Delta f \frac{\sin 2\pi(f - \Omega)\tau_0}{(f - \Omega)} \right] \right\} \quad (6.26)$$

For delay times much longer than the coherence time $\Delta f \tau_0 \gg 1$, Eq. (6.26) reduces to

$$\frac{S_I(f)}{\eta^2 E_0^4} = \frac{\Delta f / \pi}{\Delta f^2 + (f - \Omega)^2} \quad (6.27)$$

which is a Lorentzian shape with a FWHM of $2\Delta f$.

6.4 Coherence cloning using OPLLs

In Chapter 2 I pointed out that the slave laser is forced to track the phase and frequency of the master laser in an OPLL. In an ideal OPLL with infinite bandwidth, the slave laser has the same phase as the master laser and thus should inherit the coherence property of the master laser. In Section 2.4 I derived the phase noise of the locked slave laser without taking into account the relative intensity noise (RIN). As a matter of fact, the RIN of the master laser could transfer to the phase variation of the slave laser through the feedback loop, particularly if the RIN of the master laser is significant within the bandwidth of the loop. Due to the gain saturation effect of semiconductor lasers, the RIN of SCLs in an OPLL is significantly lower than the residual phase noise and can be ignored. This assumption will be further justified later by our experimental observations. Taking into account the RIN of the master laser, I will derive the phase noise of the slave laser in the OPLL.

If one assumes that the master laser has a power of $P_m = P_{m0}(1+r)$ where r

represents the RIN, and that the slave laser has a power of P_s , the feedback current reflecting the phase error is

$$i(t) = R_{pd} \sqrt{P_{m0}(1+r)P_s} \sin \phi_e(t) \quad (6.28)$$

where R_{pd} is the responsivity of the photodetector, and $\phi_e = \phi_m - \phi_s$ is the differential phase error between the master laser and the slave laser. ϕ_e can be written as the sum of a steady state value and the fluctuation, i.e., $\phi_e = \phi_{e0} + \phi_e^n$. Assuming small errors $r, \phi_e^n \ll 1$, one can expand Eq. (6.28) to first order

$$i(t) = K_{pd} \left[\sin \phi_{e0} \cdot \left(1 + \frac{r(t)}{2} \right) + \cos \phi_{e0} \cdot \phi_e^n(t) \right] \quad (6.29)$$

where K_{pd} is the photodetector gain. The constant term $K_{pd} \sin \phi_{e0}$ compensates for the free-running frequency difference between the master laser and the slave laser. Using Eq. (6.29) one can perform a small signal noise analysis similar to the analysis in Section 2.4. Fig. 6.2 is a schematic diagram of the small signal noise propagation in OPLLs. Here the shot noise of the photodetector is ignored. In addition to the phase error signal $K_{dc} \cos \phi_{e0} \cdot \phi_e^n(t)$, another term, $K_{dc} \sin \phi_{e0} \cdot r(t)/2$, is added due to the RIN of the master laser. The closed loop noise relation can be obtained as

$$\phi_s(s) = \phi_s^n(s) + G_{op} \cos \phi_{e0} \cdot [\phi_m(s) - \phi_s(s)] + G_{op} \sin \phi_{e0} \cdot r(s)/2 \quad (6.30)$$

where the open loop gain is defined as $G_{op} = K_{dc} F_f(s) F_{FM}(s) \exp(-s\tau_d)/s$, and K_{dc} is a constant representing the DC loop gain. After some algebra one obtains

$$\phi_s(s) = \phi_m \cdot \frac{G_{op} \cos \phi_{e0}}{1 + G_{op} \cos \phi_{e0}} + \phi_s^n \cdot \frac{1}{1 + G_{op} \cos \phi_{e0}} + \frac{r(s)}{2} \frac{G_{op} \sin \phi_{e0}}{1 + G_{op} \cos \phi_{e0}} \quad (6.31)$$

The PSD of the phase noise of the locked slave laser is thus

$$S_\phi^s = S_\phi^m \cdot \left| \frac{G_{op} \cos \phi_{e0}}{1 + G_{op} \cos \phi_{e0}} \right|^2 + S_\phi^{s,fr} \cdot \left| \frac{1}{1 + G_{op} \cos \phi_{e0}} \right|^2 + \frac{S_{RIN}^m}{4} \left| \frac{G_{op} \sin \phi_{e0}}{1 + G_{op} \cos \phi_{e0}} \right|^2 \quad (6.32)$$

where $S_{\phi}^{s,fr}$, S_{ϕ}^m , and S_{RIN}^m , are respectively, the PSD of the phase noise of the free-running slave laser, the master laser, and the RIN of the master laser. The PSD of the frequency noise is simply $S_v(f) = f^2 S_{\phi}(f)$.

Comparing with the phase noise of the locked slave laser derived in Section 2.4, in Eq. (6.31) and Eq. (6.32) contain an additional term, due to the RIN of the master laser. In general, the steady state phase error ϕ_{e0} is not zero and the RIN-induced residual phase noise needs to be carefully evaluated.

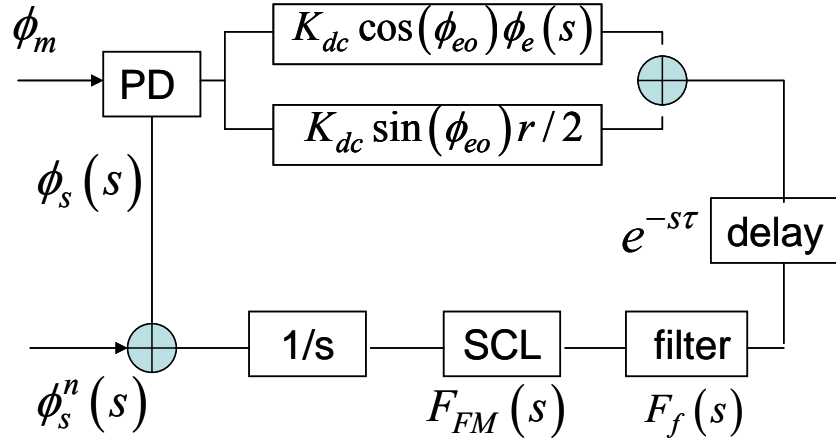


Fig. 6.2 Small signal noise propagation in an OPLL with the RIN of the master laser being considered

ϕ_m : phase of the master laser

ϕ_s : phase of the slave laser

ϕ_s^n : free-running phase noise of the slave laser

K_{dc} : loop DC gain

ϕ_{e0} : steady state differential phase error

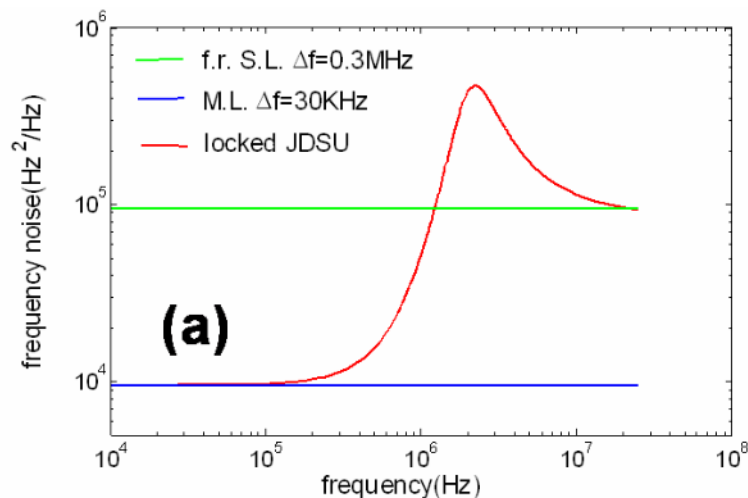
$\phi_e(s)$: small signal differential phase error

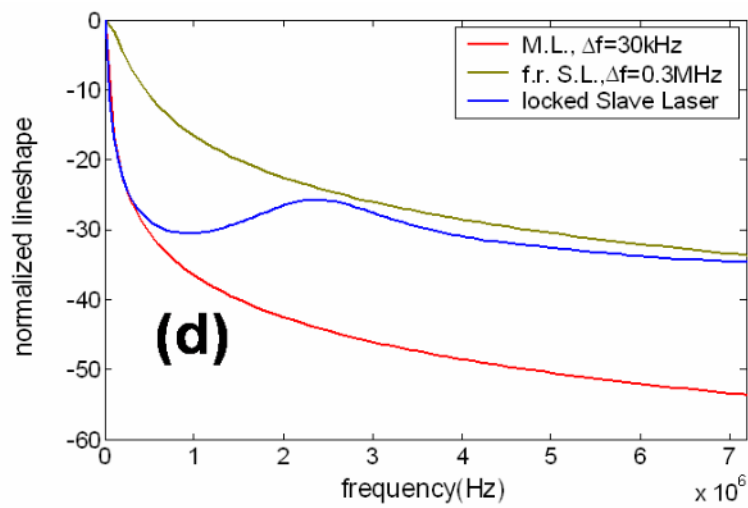
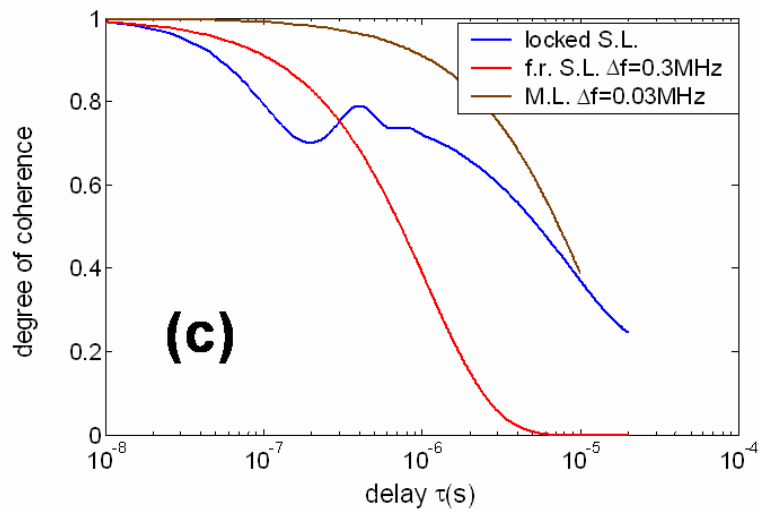
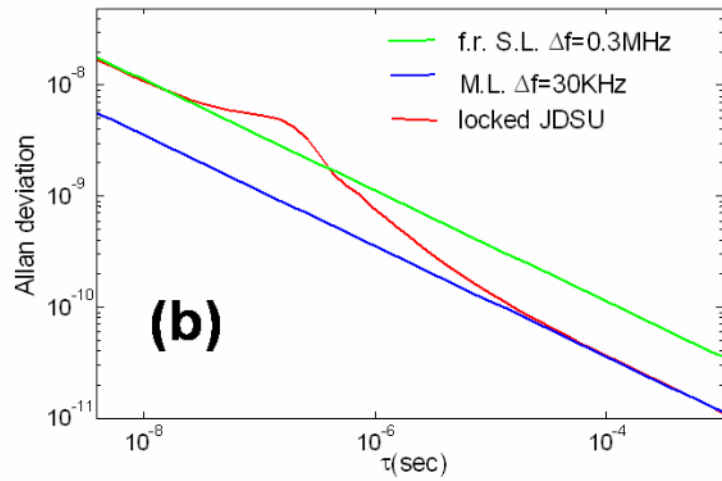
r : relative intensity noise of master laser

$F_f(s)$: normalized transfer function of the loop filter

$F_{FM}(s)$: normalized transfer function of the current-frequency modulation response of the semiconductor laser

I will use the JDSU DFB laser as an example to simulate the frequency noise of a slave laser phase locked to a narrow linewidth master laser. For the purpose of simplicity, I assume that the frequency noises of both the master laser and the slave laser are white Gaussian and the RIN of the master laser can be ignored. The current-frequency modulation response of the JDSU laser obtained in section 3.1.2 is used in the simulation. In Fig. 6.3(a) the frequency noise of a free-running JDSU laser, a narrow linewidth master laser, and the locked JDSU laser are plotted. The frequency noises of the free-running lasers are assumed to be white Gaussian. In Fig. 6.3(b)-(d) the corresponding Allan deviation, degree of coherence and single-sided lineshape are also shown. The frequency noise of the JDSU laser tracks that of the master laser within the bandwidth of the loop, as does the Allan deviation, the degree of coherence, and lineshape. For frequencies bigger than the loop bandwidth, the frequency noise goes back to the free-running level and is even amplified at a few MHz, due to the insufficient phase margin of the feedback loop.





M. L.: master laser; S. L.: slave laser; f.r.: free-running

Fig. 6.3(a) Frequency noise, (b) Allan deviation, (c) degree of coherence and (d) single-sided lineshape of the free-running and phase locked JDSU DFB laser. White frequency noise is assumed for the free-running master and slave lasers. In the simulation I have assumed a loop gain margin of $G_{mg}=10\text{dB}$ and used the FM response of the JDSU laser obtained in Section 3.1.2.

6.5. Experimental measurement

In this section, I will present the experimental measurement of the relative intensity noise (RIN), the frequency noise, and the lineshape of the master laser, the free-running slave laser and the locked slave laser. To measure the RIN, the optical signal is fed into a photodetector, whose output is then measured with a RF spectrum analyzer. The lineshape is measured using the delayed self-heterodyne interferometer displayed in Fig. 6.1. A similar setup is used to measure the frequency noise where the frequency shifter is removed and the delay length of the fiber is much shorter than the coherence length of the laser.

6.5.1 Measurement of the Agilent laser

6.5.1.1 RIN of the Agilent laser

I first measure the RIN of the Agilent laser, which will be used as the master laser to lock the JDSU DFB laser. Fig. 6.4(a) shows the measured RIN of the Agilent laser. The Agilent tunable laser is an external cavity semiconductor laser of relatively long cavity length and the RIN is significant from a few hundreds of kHz to a few MHz due to the relaxation resonance effect[39, 90].

I have pointed out in Section 6.4 that the RIN of the master laser can transfer to the frequency noise of the slave laser through the feedback loop. One can use Eq. (6.32) to evaluate the residual frequency noise of the locked slave laser due to the RIN of the master laser, and compare it with the residual frequency noise due to the free-running

frequency noise of the slave laser. In the calculation I use $\sin \phi_{e0} = 1$ for an upper bound estimation. I also use the JDSU DFB as the slave laser and assume that it has a white frequency noise corresponding to a FWHM of 0.3MHz. The results are plotted in Fig. 6.4(b). As can be seen, the blue curve is orders of magnitude lower than the red curve. Thus the residual frequency noise coupled from the RIN of the Agilent laser can be neglected.

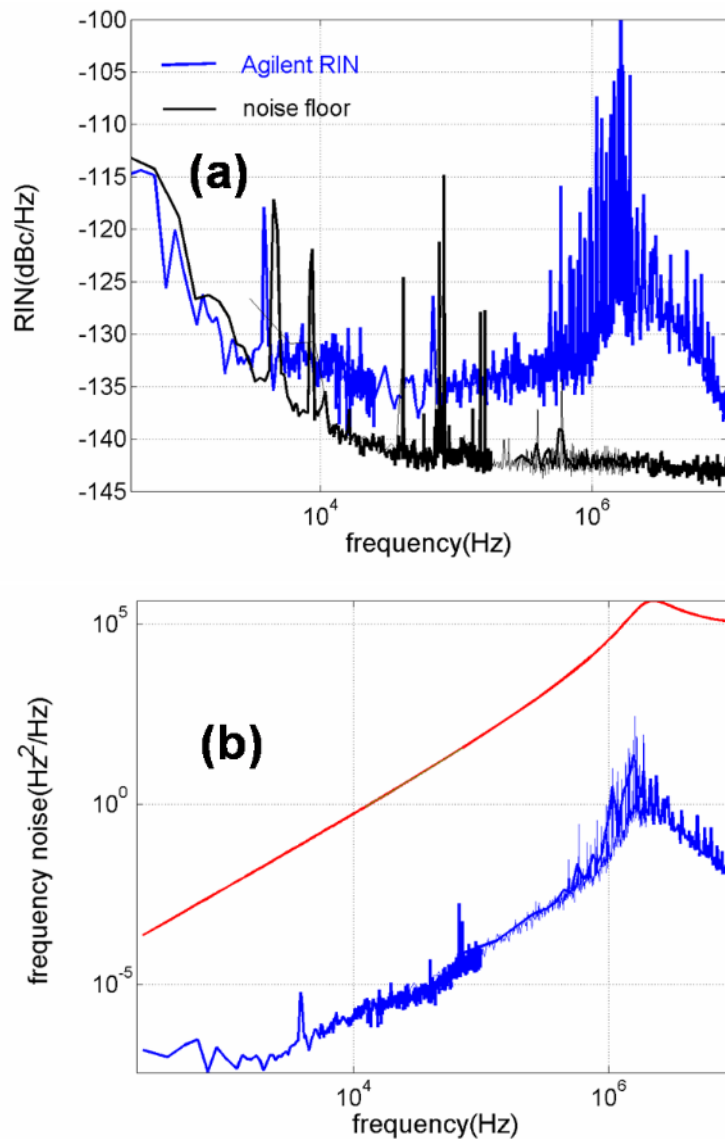


Fig. 6.4(a) Measured RIN of the Agilent laser. The black curve is the instrument noise floor. (b) Comparison of the residual frequency noise of the locked slave laser due to

the free-running noise of the slave laser (red curve) and the RIN of the Agilent laser (blue curve). In the calculation I have used Eq. (6.32) and assumed that the slave laser possesses a FWHM of 0.3MHz.

6.5.1.2 Frequency noise of the Agilent laser

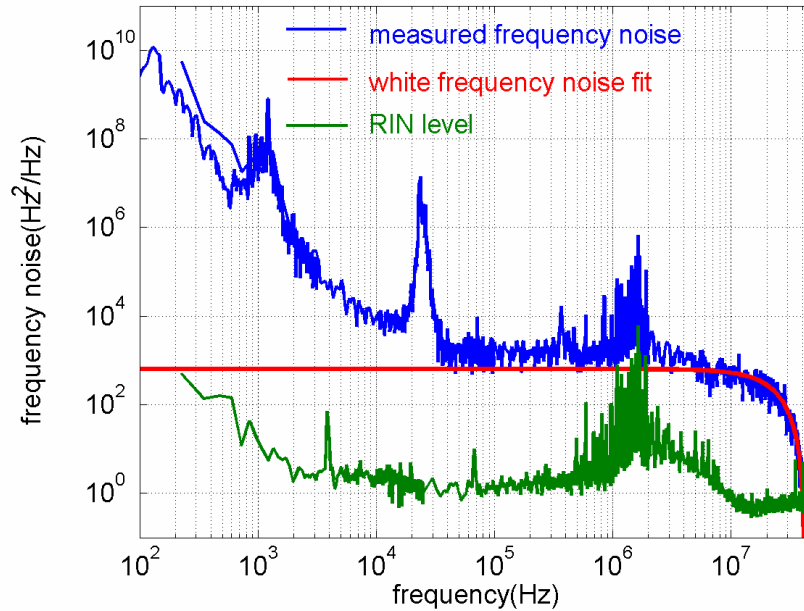


Fig. 6.5. Measured frequency noise (blue curve) of the Agilent laser. The red curve is a theoretical fitting assuming a white frequency noise corresponding to 2kHz FWHM linewidth. The dip at about 40MHz is given by the free-spectral-range of the Mach Zehnder interferometer of ~ 5 m differential delay. The green curve represents the contribution of the RIN in the frequency noise measurement.

To measure the frequency noise of the Agilent laser I use a Mach Zehnder interferometer with a differential delay of ~ 5 m. The blue curve in Fig. 6.5 is the measured frequency noise $S_\nu(f)$ (Hz^2/Hz) after the calibration. The red curve is a theoretical fit using Eq. (6.22), assuming a white frequency noise corresponding to a FWHM of 2kHz. In deriving Eq. (6.22), I have ignored the intensity noise. To consider the intensity noise one can

modify the quadrature-biased interferometer output (Eq. (6.22)) to

$$S_I(f)/(2\eta E_0^2)^2 = S_{RIN}(f) + 4\pi^2\tau_0^2 \sin^2(f\tau_0)S_V(f) \quad (6.33)$$

Eq. (6.33) indicates that the calibrated frequency noise shown in Fig. 6.5 is actually the summation of the RIN $S_{RIN}(f)$ multiplied by a factor of $1/(4\pi^2\tau_0^2)$, and the frequency noise $S_V(f)$ multiplied by a factor of $\sin^2(f\tau_0)$. Using the measured RIN shown in Fig. 6.4(a), I also calculate the normalized RIN $S_{RIN}(f)/4\pi^2\tau_0^2$ and plot it in Fig. 6.5. As can be seen, the contribution of the RIN is at least two orders of magnitude lower than the measured frequency noise. Thus one can neglect the effect of the RIN in the frequency noise measurement.

The frequency noise of the Agilent laser at frequency above ~ 30 kHz is mainly white with significantly higher noise between ~ 100 kHz and ~ 10 MHz due to the intensity-frequency noise coupling. At frequency lower than 30kHz, higher order frequency noises such as f^{-1} and f^{-2} noises dominate.

6.5.1.3 Lineshape of the Agilent laser

To measure the lineshape I use the delayed self-heterodyne interferometer. Due to the frequency jitter, the measured lineshape and linewidth depend on the differential delay time of the interferometer[32, 82]. With a fiber delay of 500m, the mixed signals are still coherent and interference fringes can be seen on the spectrum. When the delay length is increased to 4km, the signals are almost incoherent. Fig. 6.6 gives the measured lineshape(green curve) of the Agilent laser with a fiber delay of 4km. The 20dB full width is about 0.46MHz.

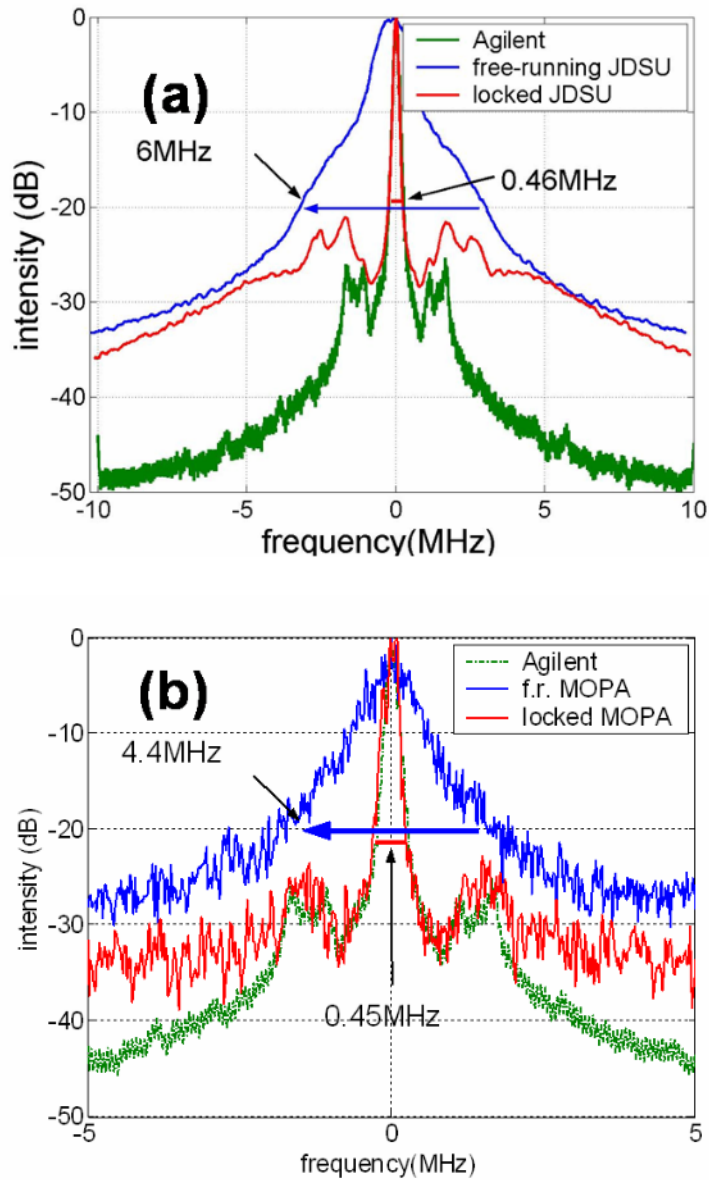


Fig. 6.6 Delayed self-heterodyne lineshape measurement of the master laser, the free-running slave laser, and the locked slave laser. (a) A JDSU DFB is used as the slave laser and (b) A QPC MOPA is used as the slave laser. The master laser is an Agilent tunable laser.

6.5.2 Measurement of the free-running and locked JDSU DFB laser

I repeated similar measurements on the JDSU DFB laser. The measured RIN and

frequency noise of the free-running JDSU DFB laser are plotted in 6.7(a) and 6.7(b). The RIN measurement is limited by the instrument noise floor at frequency smaller than $\sim 1\text{MHz}$ and by the shot noise at higher frequencies. As seen in Fig. 6.7(b), the frequency noise agrees well with the theoretical fit assuming a white frequency noise corresponding to a FWHM of 0.3MHz . The lineshape is measured with the same interferometer of 4km differential delay and plotted by the blue curve in Fig. 6.6(a).

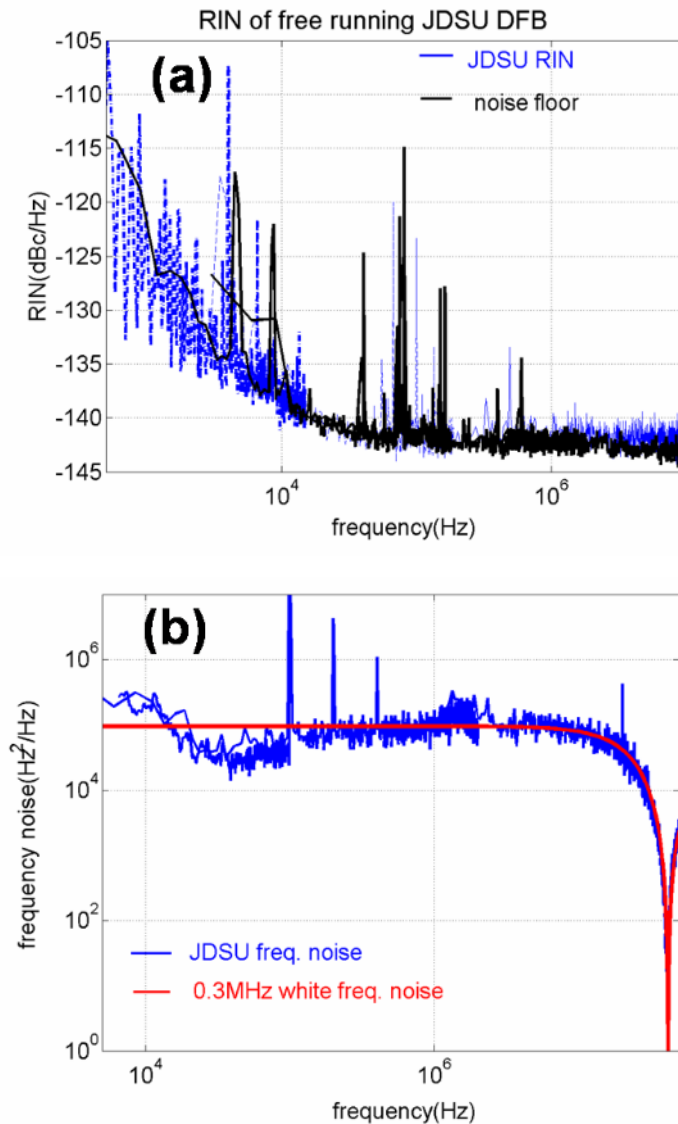


Fig. 6.7 Measured (a) RIN and (b) frequency noise of the free-running JDSU DFB laser. In (b), the red curve is a theoretical fitting assuming a white frequency noise corresponding to a FWHM linewidth of 0.3MHz .

In next phase locked the JDSU laser to the Agilent laser and measured its RIN, frequency noise, and lineshape. The RIN of the locked JDSU laser is similar to the free-running case and its measurement is limited by the instrument and shot noise floor. The low RIN justifies the assumption in deriving Eq. (6.28) that the RIN of the slave laser can be neglected when one analyze the residual frequency noise of the slave laser in the OPLLs.

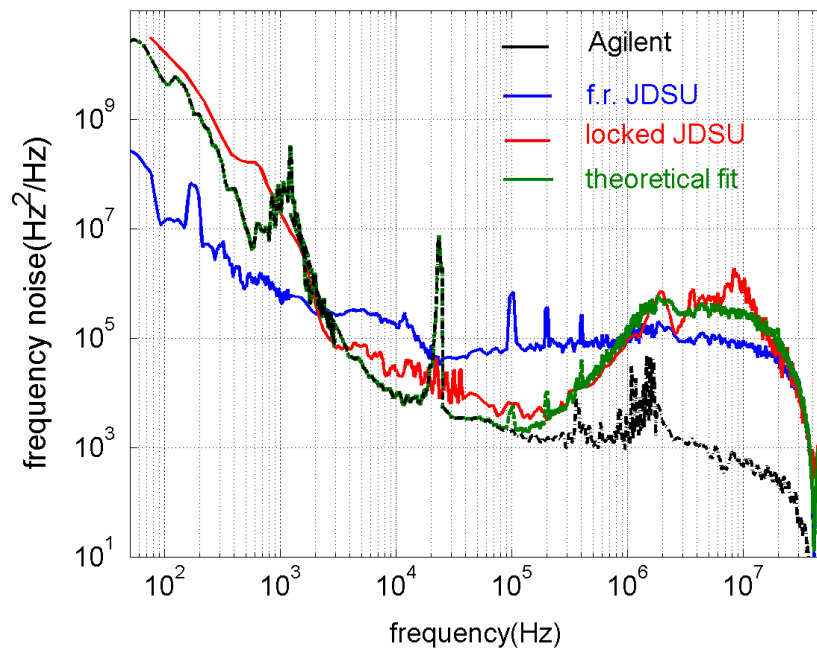


Fig. 6.8 Comparison of the frequency noise of the Agilent master laser (black curve), the free-running (blue curve), and the phase locked JDSU slave laser (red curve). The green curve is a theoretical fitting of the frequency noise of the locked JDSU laser using the measured frequency noise of the free-running JDSU laser, the Agilent laser, and the loop transfer function. The measured data shown here are smoothed with a 5 points moving average algorithm.

The measured frequency noise of the locked JDSU laser is plotted in Fig. 6.8 and compared to the free-running JDSU laser and the Agilent laser. As can be seen, the frequency noise of the locked slave laser follows that of the master laser for frequencies

smaller than $\sim 100\text{kHz}$. The frequency noise is reduced between $\sim 2\text{kHz}$ and $\sim 1\text{MHz}$ and increased for frequency less than $\sim 2\text{kHz}$ due to the higher frequency noise of the master laser at low frequency. It is also amplified between 1MHz and 20MHz due to the insufficient phase margin of the loop.

With the knowledge of the frequency noises of the free-running JDSU laser, the Agilent master laser and the loop transfer function, one can theoretically calculate the frequency noise of the locked JDSU laser using Eq. (6.32) and compare it to the measurement. The calculation is also plotted in Fig. 6.8 by the green curve. The theoretical calculation agrees reasonably well with the measured result (red curve).

The measured lineshape of the locked JDSU laser is plotted in Fig. 6.6(a) as the red curve. Compared to the free-running case (blue curve), the lineshape of the locked JDSU laser is significantly narrowed within the bandwidth of the OPLL ($< 1\text{MHz}$). The 20dB full width is reduced from 6MHz to 0.46MHz . The linewidth of the locked slave laser is limited by the linewidth of the master laser.

6.5.3 Measurement of the NP fiber laser and the locked JDSU laser

Fiber lasers are well known for their narrow linewidth and low phase noise[72]. In this section I will use a spectrally stabilized NP photonics fiber laser as the master laser to lock the JDSU DFB laser, then measure and compare their noise properties.

I first measured the RIN, the frequency noise, and the lineshape of the NP fiber laser. Fig. 6.9(a) is the measured RIN of the NP fiber laser under the free-running mode operation (red curve) and the RIN suppression mode operation (blue curve). The spectral peak at $\sim 1\text{MHz}$ is caused by the relaxation resonance effect[39, 90] of the fiber laser. The black curve is the instrument noise floor. I further use Eq. (6.32) to calculate and compare the residual frequency noise of the locked slave laser due to its free-running frequency noise and to the RIN of the NP fiber laser under the RIN suppression mode operation.

The results are plotted in Fig. 6.9(b). The RIN-induced residual frequency noise is significantly lower and can be neglected.

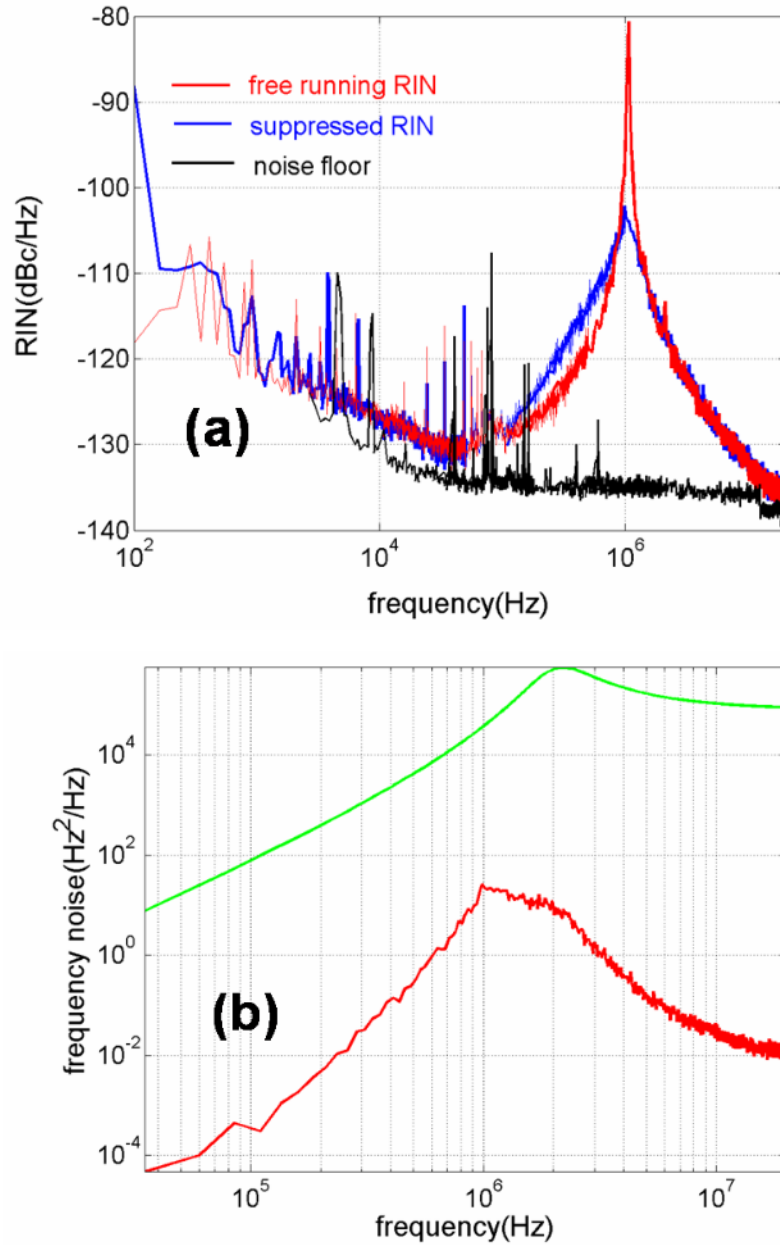


Fig. 6.9(a) Measured RIN of the NP fiber laser under both the free-running and the RIN suppression modes. (b) Calculated residual frequency noise of the locked slave laser (JDSU DFB) due to its free-running frequency noise (green curve) and to the RIN of the master laser (red curve). A white frequency noise corresponding to a FWHM of 0.3MHz

is assumed for the free-running slave laser.

I then use a fiber Mach-Zehnder interferometer to measure the frequency noise of the NP fiber laser. Because the fiber laser has significantly lower frequency noise compared to the Agilent laser and the JDSU DFB laser, a differential delay of $\sim 50\text{m}$ has to be used to enhance the sensitivity of the interferometer. However, the small free spectral range of the interferometer, combined with the frequency jitter of the NP laser, makes it very difficult to bias the Mach Zehnder interferometer at the quadrature point long enough to take a measurement of the frequency noise spectrum with a small enough resolution and video bandwidth. To solve this problem, I measure a large number of traces of the frequency noise spectrum at random times and average these traces. In order to prove that this method works, I expand Eq. (6.20) to

$$I/(2\eta E_0^2) = 1 + \cos \omega_0 \tau_0 \cos \Delta\phi(t, \tau_0) - \sin \omega_0 \tau_0 \sin \Delta\phi(t, \tau_0) \quad (6.34)$$

Under the small differential phase error assumption $\Delta\phi(t, \tau_0) \ll 1$, one keeps only the last term of Eq. (6.34), which leads to the relation Eq. (6.22) at the quadrature point $\omega_0 \tau_0 = (N + 1/2)\pi$. In general $\omega_0 \tau_0$ varies with time and can be any value due to the frequency jittering of the laser and the variation of the interferometer, and the measured frequency noise spectrum has an additional multiplication factor $\sin^2(\omega_0 \tau_0)$. If one takes the average of a large number of traces, it is equivalent to averaging the factor $\overline{\sin^2(\omega_0 \tau_0)} = 1/2$. Thus one only needs to calibrate the averaged frequency noise spectrum by a factor of 2 to get the right answer. However care must be taken if the small differential phase error assumption $\Delta\phi(t, \tau) \ll 1$ is not satisfied, since the second term in Eq. (6.34) is highly nonlinear away from the quadrature point, and can spread the spectral energy of the frequency noise and skew the measurement. An example of such a case will be given later.

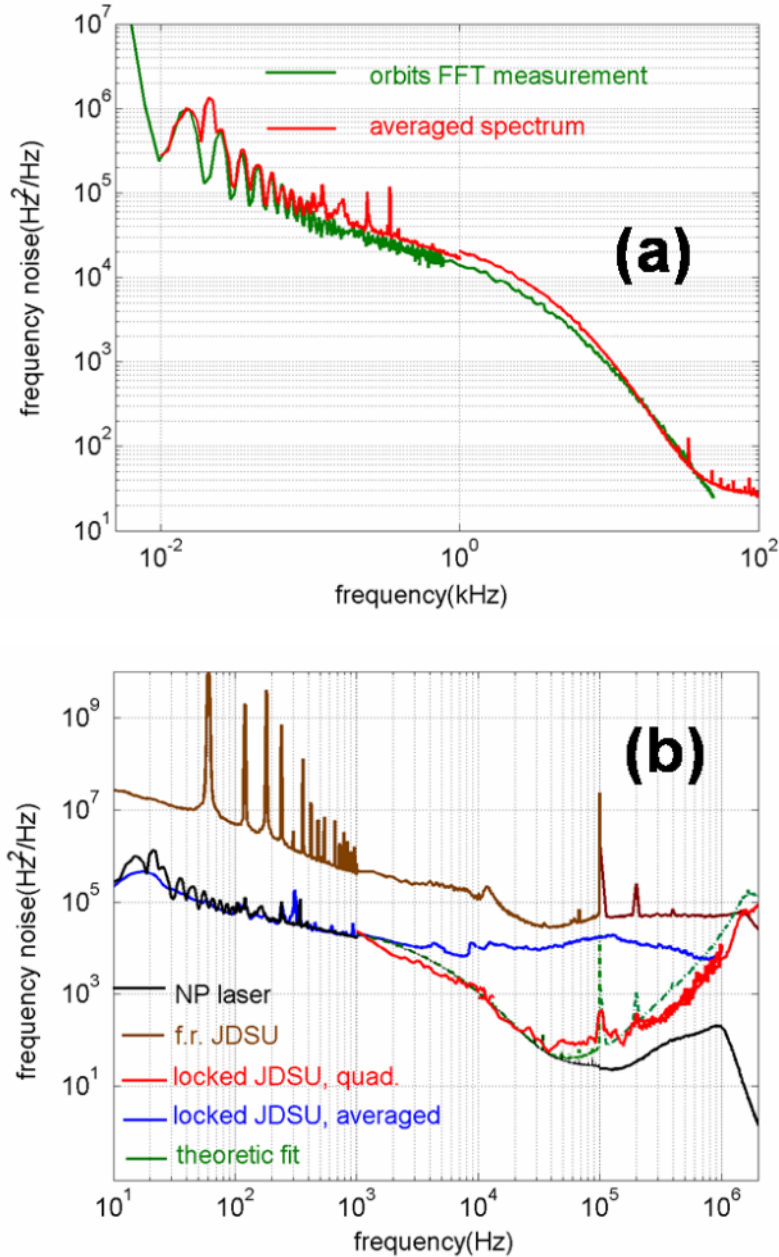


Fig. 6.10(a) Comparison of the measured frequency noises of the NP fiber laser. The green curve is measured in Orbitlightwave. Inc using a real-time spectrum analyzer, by taking the FFT of the output of the Mach Zehnder interferometer near the quadrature point. The red curve is measured by averaging a large number of traces taken by a sweep-filter type spectrum analyzer. In both measurements the differential delay of the interferometer is ~ 50 m. (b) Comparison of the measured frequency noise of the master laser(NP fiber laser), the free-running and the locked JDSU laser. The red curve between

1kHz and 1MHz is measured at the quadrature point of an interferometer of 5m differential delay. The blue line is measured by averaging a large number of the frequency noise spectra using an interferometer of 50m differential delay. The green curve is a theoretical fitting of the frequency noise of the locked JDSU laser using Eq. (6.32).

Using the spectrum averaging approach, I measured the frequency noise of the NP fiber laser using an interferometer of 50m and plot it in Fig. 10(a). The green curve is measured using a real-time spectrum analyzer by taking the FFT of the output of the Mach Zehnder interferometer near the quadrature point. The results of the two approaches agree well with each other between 10Hz and 100kHz. Using the same approach, I also measured the frequency noise of the NP laser, the free-running and the locked JDSU laser from 10Hz to a few MHz. They are plotted in Fig. 10(b), respectively, as the black, the brown, and the blue curves. I also measured the frequency noise of the locked JDSU laser between 1kHz and 1MHz at the quadrature point of an interferometer of 5m delay. The data is plotted as the blue curve in Fig. 10(b). Using Eq. (6.32), I also calculate the expected frequency noise of the locked slave laser and plot it as the green curve. As can be seen, the spectrum averaging approach works well at frequency lower than ~30kHz and bigger than ~800kHz. In the range 30kHz-800kHz, the measured noise level is much higher than the expected value. Instead, the measurement taken at the quadrature point is close to the expected value. This is due to the significant nonlinearity of the second term in Eq. (6.34) when the interferometer drifts away from the quadrature point. The energy of the frequency noise at higher frequency spreads out to the lower frequency range through the nonlinear effect of the interferometer. The detailed study of the phenomenon is out of the scope of this thesis.

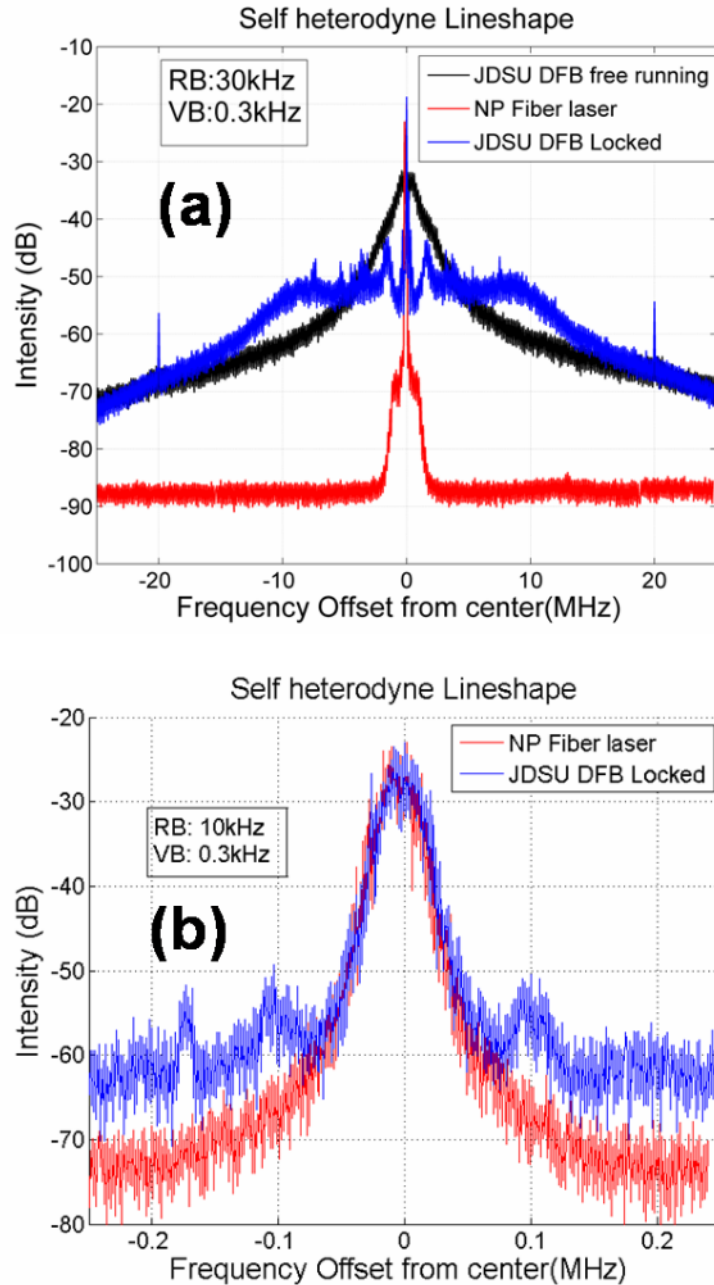


Fig. 6.11 Measured lineshapes of the master laser (NP fiber laser), the free-running and the locked slave laser (JDSU DFB) on a (a) 5MHz span and (b) 0.5MHz span

I also measured the lineshape of the NP fiber laser and the locked JDSU DFB laser. Using a delay line of 25km, the measured lineshapes of the NP fiber laser, the free-running JDSU DFB laser and the locked JDSU DFB laser are plotted and compared

in Fig. 6.11(a) on a span of 50MHz and in Fig. 6.11(b) on a span of 0.5MHz. One can see that the lineshape of the JDSU DFB laser follows that of the NP fiber laser within $\pm 50\text{kHz}$ frequency range and the 20dB full linewidth is reduced from $\sim 5\text{MHz}$ to $\sim 50\text{kHz}$. The linewidth of the locked slave laser is still limited by the linewidth of the master laser. The part of the lineshape at higher frequencies is not affected due to the limited noise correction bandwidth of the OPLL. This observation is also consistent with the frequency noise measurement shown in Fig. 10(b), where the frequency noise of the locked JDSU laser follows that of the NP laser only for frequencies lower than $\sim 50\text{kHz}$.

Conclusion

In this chapter I have studied the application of OPLL in cloning the coherence property of a low phase noise fiber laser to an inexpensive commercial semiconductor DFB laser. Compared to fiber lasers, SCLs have very low RIN but much higher frequency noise. When the SCLs are phase locked to the fiber laser, they have essentially the same frequency noise as the fiber laser, meanwhile their RIN remains very low. Nevertheless, due to the insufficient loop bandwidth limited mainly by the non-uniform current-frequency modulation response of the SCLs, the coherence property of the fiber laser can only be cloned to the SCLs within a limited bandwidth. If multisection SCLs are used to remove this barrier, one can use the OPLL technology to obtain high power laser source of both low RIN and low phase noise for a number of critical applications.